TESLA, 4/1995

Design Study of a Beam Dump for the TESLA and S-Band Test Facilities at DESY

I.S. Baishev†, M.A. Maslov†, M. Seidel

† Institute for High Energy Physics, Protvino, Russia

1. Overview

The beam dump of the TESLA test facility must be capable to absorb an average beam power of 51 kW at a beam energy of 800 MeV. Because the available space is limited, the longitudinal size of the dump should not exceed 1.4 m. As a further requirement the integral radiation leakage should not exceed 1 percent of the beam power.

The average beam power is comparable to several existing beam dumps (table 1). However, the low repetition rate of the TTF (10 bunch trains per second with a length of 800 μs each) leads to a strong instantaneous temperature rise during the passage of a macro pulse. The high beam energy per bunch train presents at least a lower limit for the beam dimensions at the surface of the dump block (or at the exit window of the beam pipe). The S-Band parameters are much more relaxed (see table 1). Two different dump designs have been under discussion - the so called sphere dump [1], [2] and the classical scheme of a solid dump block with optional spoiler [3], [4], [5].

machine	E_{beam} [GeV]	N_{mac}	P_{avg} [kW]	E_{mac} [kJ]	type of dump
SLAC	18	10^{12} (180 Hz)	500	2.8	sphere (Al H_2O) [1]
MAMI	0.84	CW	84	-	sphere (Al H_2O) [2]
SLAC	50	$5{\cdot}10^{10}$ (180 Hz)	72	0.4	solid (Al Fe) [3]
CEBAF	0.6	CW	96	-	solid (Al Cu) [4]
LEP	100	$7{\cdot}10^{12}$ (1×)	-	106	solid (Al Cu alloy) [5]
TTF	0.8	$4{\cdot}10^{13}$ (10 Hz)	52	5.1	solid (C+Al+Cu)
SBT	0.45	$6.3{\cdot}10^{12}$ (50 Hz)	27	0.54	solid (C+Al+Cu)

Table 1: Beam parameters of several machines (E_{mac} is the beam energy per macro pulse).

The sphere dump consists of a hollow cylinder which is filled with a closely packed bed of aluminum spheres. The bed of spheres is continuously cooled by circulating water. The advantage of this design is the very efficient cooling of the spheres due to the high surface to volume ratio. The sphere dump is therefore well suited for very high average beam powers. Furthermore the solution is relatively easy to manufacture and cheap. The most important disadvantage, however, is the large amount of direct power deposition in water. This leads to radiolysis and production of a considerable amount of hydrogen which must be removed by catalytic recombiners (production rate $3{\cdot}10^{-4}$ l H_2 per kJ of in water deposited power [3]). An even more unpleasant problem arises from the production of radioactive isotopes in the water cooling system. Among short living isotopes as O^{15} are some with longer lifetimes as Be^7 which could steadily built up and make the servicing of the system very complicated. On the other hand the moderate average power of the TTF and S-Band beams does not demand the usage of a sphere dump under any circumstances. An edge cooled solid dump block seems to be a better solution. Such a solid dump is usually made of a low Z material like aluminum or graphite in order to achieve a moderate energy loss per unit length. The end of the dump should be backed up with a short copper section in order to absorb the residual radiation. The outer surface of the cylinder is cooled by circulating water. The amount of direct beam power, deposited in the water, is therefore reduced by several orders of magnitude, compared to the sphere dump. For the TTF and S-Band dumps we demand that the radiation power deposition in the water is less than 40 W. The extraction of the average power presents no problem and the parameters of the SLAC design [3] with respect to the water cooling requirements can

probably be overtaken. This dump is cooled by a helical water flow channel on the radial surface with a water flow of 1.25 l/s. For a good cooling efficiency it is important to guarantee highly turbulent flow.

2. Analytical Estimate of Dump Heating and Stresses

We consider a solid dump cylinder of radius b. The incident beam initiates an electromagnetic shower in the material which leads to a certain distribution of deposited power $Q(x,y,z,t)$ in space and time. The resulting temperature distribution in the absorber block is obtained as a solution of the heat equation:

$$\frac{\partial}{\partial t}T(x,y,z,t) = \frac{\lambda}{\rho c}\nabla^2 T(x,y,z,t)+\frac{1}{\rho c}Q(x,y,z,t) \qquad (1)$$

where ρ is the density of the material,
c is the specific heat and
λ the heat conductivity.

Furthermore one has the boundary condition:

$$T\left(\sqrt{x^2+y^2}=b,t\right) \equiv T_{edge}.$$

A complete solution of (1) is possible only numerically. However, with some simplifying assumptions one can estimate the peak temperature distribution in the material for a certain power distribution. During the passage time $\tau = 800\ \mu s$ of a bunch train the temperature distribution broadens up transversally by a typical diffusion length of

$$<d> = \sqrt{D\tau} = \sqrt{\frac{\lambda\tau}{\rho c}} \approx 0.25\ \text{mm}.$$

This distance is small compared to the beam size and therefore we can assume that the instantaneous temperature rise is directly proportional to the distribution of deposited energy. After the bunch train passage the temperature distribution spreads and the temperature on the axis decays with time till the next passage. From these considerations we expect a sawtooth like behaviour of the temperature on the beam axis with time. The passage of a bunch train will cause a sudden instantaneous temperature rise of ΔT_{inst}. On the other hand in the case of a CW beam with an assumed average power of the real beam we would expect an equilibrium temperature of $T_{edge} + \Delta T_{eq}$. A conservative estimate of the maximum temperature is therefore

$$T_{max} \le T_{edge} + \Delta T_{inst}(r=0) + \Delta T_{eq}(r=0).$$

The value of ΔT_{inst} is simply given by the assumption that the whole beam energy is deposited in the volume of the beam cone:

$$\Delta T_{inst}(r) = \frac{q(r)\cdot n_{mac}}{\rho\cdot c} \qquad (2)$$

where $q(r)$ is the transversal distribution of deposited energy per incident particle and n_{mac} the number of particles per macro pulse. From (2) one can conclude that a material with a high

specific heat is desirable. On the other hand the coefficient $q/\rho \propto \left(\frac{dE}{dz}\right)/\rho$ is nearly constant for different materials.

For the calculation of ΔT_{eq} we have to solve equation (1) in the stationary case $\partial/\partial t \equiv 0$. We neglect the longitudinal dependence of q, longitudinal heat transport and assume a round beam which allows the use of cylindrical coordinates. Then we obtain from (1):

$$n_{mac}\, \nu_{mac}\, q(r) \;=\; -\lambda \frac{1}{r}\frac{\partial}{\partial r} r \frac{\partial}{\partial r}\, \Delta T_{eq}(r), \qquad (3)$$

where ν_{mac} is the bunch repetition rate in s^{-1}. Equation (3) can be solved by twice integration, yielding the solution

$$\Delta T_{eq}(r) \;=\; \frac{\nu_{mac} n_{mac}}{\lambda} \int_{s=r}^{b} \frac{ds}{s} \int_{u=0}^{s} q(u)\, u\, du \qquad (4)$$

with b the outer radius of the dump block. The radial distribution of deposited power can be taken from a shower simulation for each longitudinal slice of the dump. Then the integrals in (4) are replaced by sums in the following way:

$$T_{k_r} \;=\; T_{k_b} \;+\; \nu_{mac} n_{mac} \sum_{k=k_r}^{k_b} \frac{\Delta r}{r_k \lambda_k} \sum_{l=0}^{k} r_l \cdot q_l \cdot \Delta r, \qquad (5)$$

where T_{k_b} is the temperature at the radial border of the cylinder and k_r is the index of the radial bin in which the temperature shall be determined, Δr is the bin width. If the summation is carried out successively from the outer radius $k = k_b$ towards $k = 0$ one can determine for each step the correct value of the thermal conductivity λ_k which is in general a function of the materials temperature.

Another method which helps to gain more insight in the physical dependencies is to insert an empirical fit-function for the radial distribution $q(r)$ of deposited energy per particle and per volume in an electromagnetic shower. A good approximation is given by the parameterization of Grindhammer [6]:

$$q(r) \;=\; \left(\frac{dE}{dz}\right) \frac{R^2}{\pi\left(r^2 + R^2\right)^2}, \qquad (6)$$

where $\left(\frac{dE}{dz}\right)$ is the energy loss in the shower per unit length, per incident particle and R gives a typical transverse shower width. If we consider a Gaussian beam with rms-width σ then it holds at the entrance of the dump approximately $R(z=0) \approx \sqrt{2}\sigma$. It should be emphasized that $q(r=0)$ and therefore the instantaneous heating depend strongly on the beam size as σ^{-2}. As the shower develops inside the material the values of R and $\left(\frac{dE}{dz}\right)$ have to be determined from the results of a shower code. In Fig. 1 an example for a fit of (6) to a radial shower distribution, obtained from a GEANT simulation, is shown.

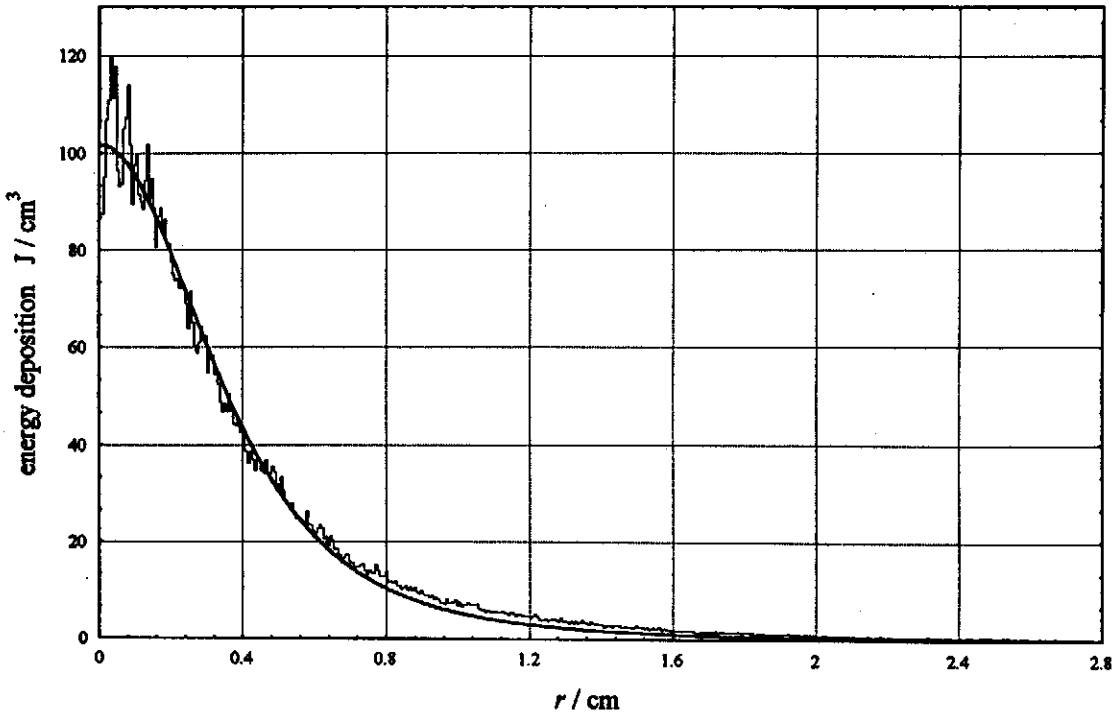

Fig. 1: Example of a fit to the transversal distribution of energy deposition per volume and per bunch train at the shower maximum.

Inserting (6) in (4) yields a closed expression for the equilibrium temperature distribution:

$$\Delta T_{eq}(r) = \left(\frac{dE}{dz}\right)\frac{n_{mac}v_{mac}}{4\pi\lambda} ln\left(\frac{R^2+b^2}{R^2+r^2}\right). \qquad (7)$$

From (7) it can be seen that for a low equilibrium temperature it is desirable to use a material with low $\left(\frac{dE}{dz}\right)$ and high λ. The equilibrium temperature depends only weakly on the beam size because R is contained in the logarithmic term. So we obtain in a conservative approach for the maximum temperature on the beam axis (note that $\left(\frac{dE}{dz}\right)$ and R depend on z):

$$T_{max} \leq T_{edge} + \left(\frac{dE}{dz}\right)\frac{n_{mac}}{\pi}\left(\frac{1}{\rho c R^2} + \frac{v_{mac}}{4\lambda} ln\left(1+\frac{b^2}{R^2}\right)\right). \qquad (8)$$

The maximum temperature should stay well below the melting point of the absorber material. Furthermore one has to consider stresses which are induced due to the raised temperatures and which may deform or even destroy the material and are therefore limiting factors for beam power and beam size. In case of a cylindrical geometry the stresses can be calculated with analytical formulae [7]. A stress is a vector force per unit area and in cylindrical coordinates the stress field is given by three components in the directions of the unit vectors e_r, e_φ, e_z. The following formulae hold for a cylinder with not prevented expansion in longitudinal and transversal direction.

$$\sigma_r = \frac{\alpha E}{1-\nu}\left(\xi(b)-\xi(r)\right)$$

$$\sigma_\varphi = \frac{\alpha E}{1-\nu}\left(\xi(b)+\xi(r)-T(r)\right)$$

$$\sigma_z = \frac{\alpha E}{1-\nu}\left(2\xi(b)-T(r)\right), \qquad (9)$$

where α - coefficient of lin. thermal expansion,
ν - Poisson's ratio (≈ 0.26 for graphite, 0.33 for aluminum),
E - elastic modulus,
$\xi(x) = \frac{1}{x^2}\int_{r=0}^{x} T(r)\,r\,dr$.

Plastic deformations can occur in principle if the stress exceeds the so called 0.2 % yield strength $\sigma_{0.2}$. For estimating allowed stresses the difference between the three components is important. In our case we use the equivalent stress, given by the so called v. Mises criterion, which is computed from the differences of the three components (see the definition in chapter 3.3).

From the above considerations we conclude that desirable material properties are: high $\sigma_{0.2}$, small α and small E. Different materials can be compared by a typical allowed temperature difference $\Delta T_m = \frac{2\sigma_{0.2}}{3\alpha E}$.

3. Numerical Simulation of Beam Dumping

The incident beam of high energy electrons initiates an electromagnetic shower (EMS) in the dump material. The components of the EMS are electrons, positrons and photons. Other particles like neutrons, protons etc. can be produced in interactions of high energy photons with nuclei but almost all the EMS energy is deposited in material via ionization and excitation of atoms by the charged EMS components. The space distribution of EMS energy deposition depends strongly on the materials atomic number and density. Combined with the beam time structure it defines the primary heat source. The resulting temperature distribution depends on the thermal properties of the material and on the cooling conditions.

Nuclear interactions of photons and neutrons produce various radioactive isotopes both in the dump material and in the coolant. High absorbed doses of radiation can lead to radiation damage of materials especially when organic materials are used as electrical insulation or lubricants.

3.1 Shower Simulations

Looking at the above general considerations, the mechanical and thermal properties of aluminum, graphite and copper make them the best candidates for the dump material. The results of EMS simulations, generalized in [8], can be used to estimate the required dump dimensions. The length L of an infinitely wide homogeneous dump, absorbing 99% of the incident electron energy E_0 , can be estimated by the following expression:

$$L = \left(1.52\cdot\ln(E_0/\mathrm{MeV}) - 4.1\cdot\ln(E_c/\mathrm{MeV}) + 17.6\right)\cdot X_r,$$

where E_c is the critical energy and X_r - the radiation length of the dump material. The radius R of an infinitely long cylinder absorbing 99 % of incident energy must be equal to approximately 5 Moliere lengths $R_M = (21.2\ \text{MeV}) \cdot X_r / E_c$.

As shown above the maximum temperature in the dump is proportional to the maximum of the longitudinal distribution of deposited energy $(dE/dz)_m$. The values of L, R and $(dE/dz)_m$ along with X_r, E_c, R_m and density ρ are presented in table 2.

	ρ [g cm^{-3}]	X_r [cm]	E_c [MeV]	R_m [cm]	L [cm]	R [cm]	$(dE/dz)_m$ [MeVcm^{-1}]
Graphite	1.71	25.1	75.9	7.0	250.	35.	8.5
Aluminum	2.70	8.89	40.0	4.7	112.	24.	16.5
Copper	8.96	1.435	18.8	1.6	23.	8.	92.

Table 2: Properties of the dump materials.

The three materials are arranged in the dump in descending order with respect to the radiation length. Computer simulations of the EMS are necessary to optimize the sizes of the dump sections but crude estimations can be done using universal longitudinal distributions from [8]. The criterion can be an approximate equality of $(dE/dz)_m$ in each section. Under this criterion the length of the graphite section should be approximately 80 cm to 100 cm, aluminum - 30 cm to 40 cm, and copper - 10 cm to 15 cm. Therefore the requirement of 140 cm total length can be satisfied. The outer radius of such a dump should be approximately 25 cm and the graphite core radius should be approximately 10 cm.

The Monte-Carlo code RAINMC [8] was used for the electromagnetic shower simulations. Several runs were made to adjust the lengths of the dump sections. Finally the lengths have been defined as 90 cm for the graphite core, 35 cm for the aluminum section and 15 cm for the copper backing (see fig. 2). Fig. 3 shows the longitudinal distribution of (dE/dz).

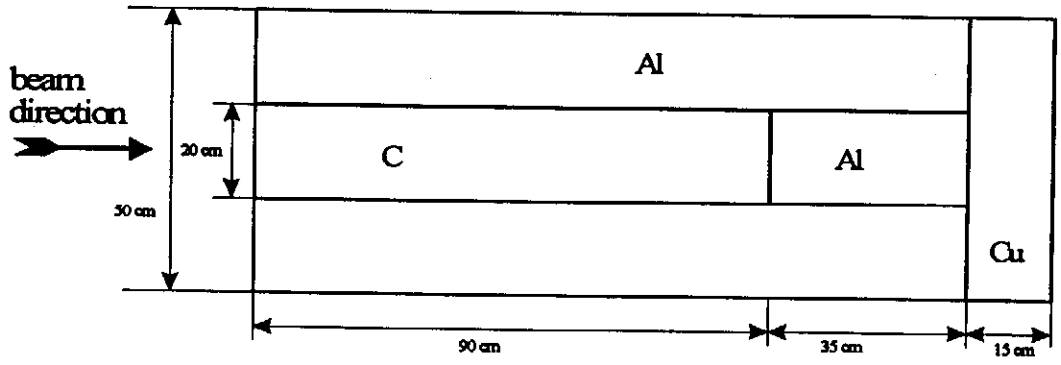

Fig. 2: Longitudinal section of the beam dump.

The maximum values of (dE/dz) are for the graphite section: $(dE/dz)_m = 8.3$ MeV/cm, for the aluminum section $(dE/dz)_m = 7.2$ MeV/cm, and for the copper section $(dE/dz)_m = 8.9$ MeV/cm. The space distribution of energy deposition density used in the below thermal and corresponding mechanical stress analysis is tabulated in the Appendix.

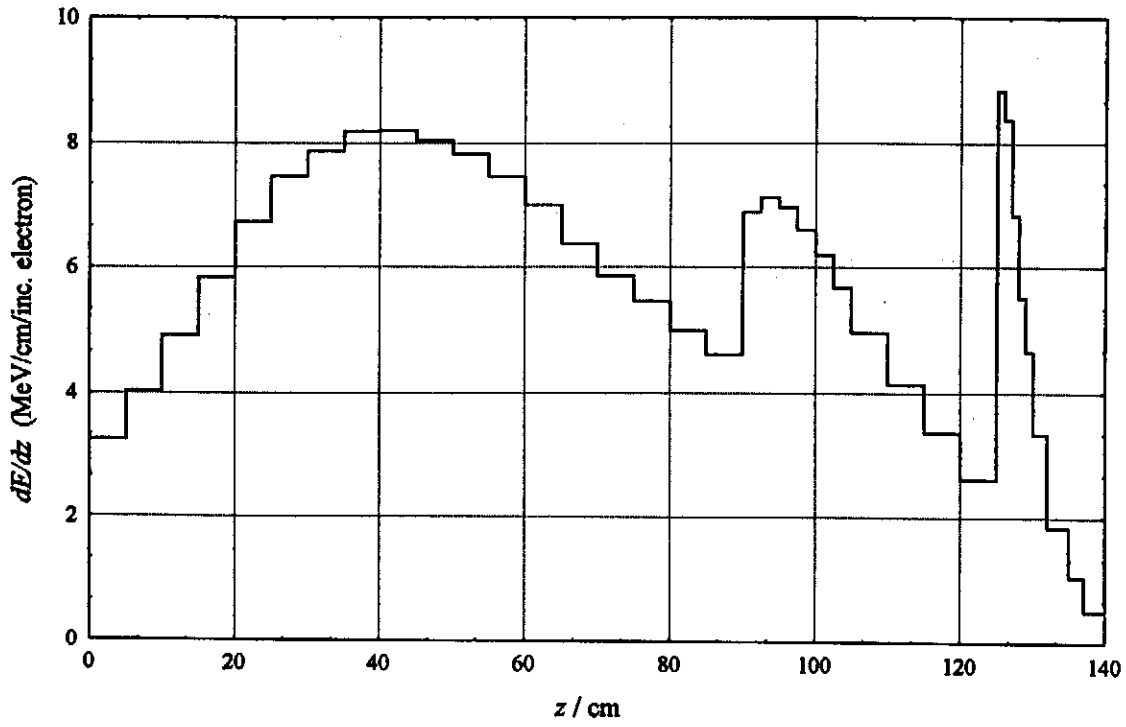

Fig. 3: Longitudinal distribution of deposited energy per incident electron.

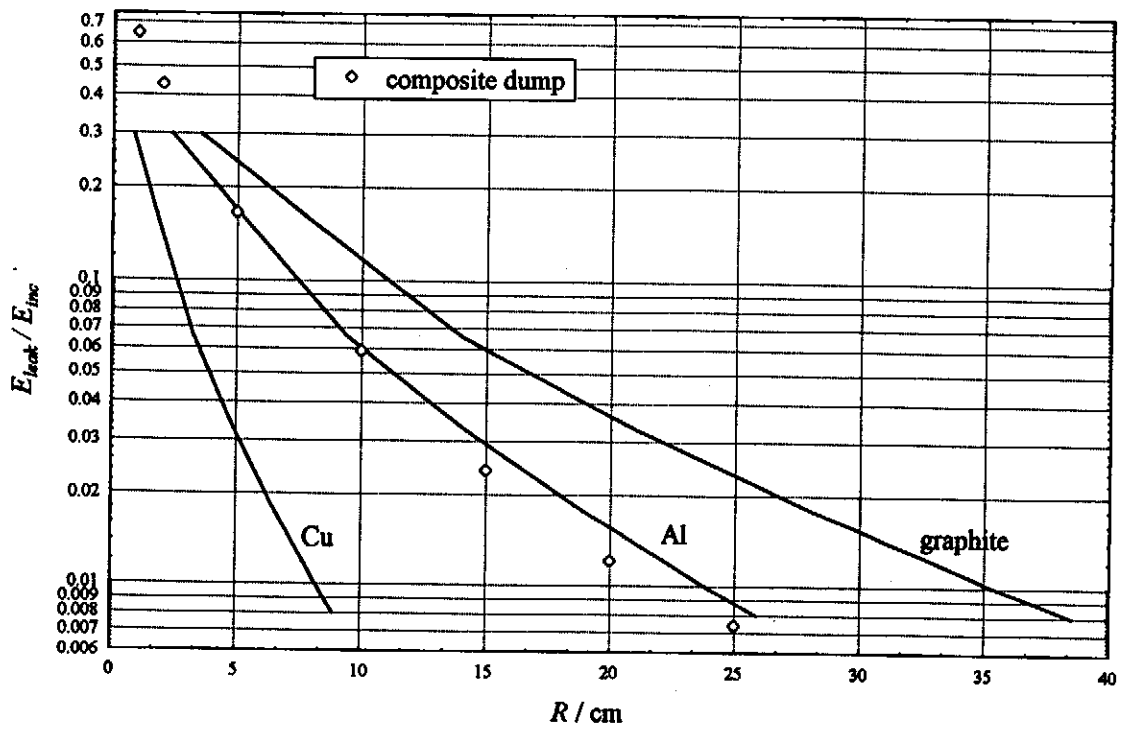

Fig. 4: Relative transverse loss for different dump materials as a function of the dump cylinder radius.

The dependence of the electron/photon energy leakage through the lateral surface of the dump on the dump radius R is illustrated in fig. 4. The simulation results for the composite dump are presented along with the results for homogeneous cylinders extracted from [8]. It can be seen that the composite dump behaves like an aluminum dump. The percentage of incident energy

corresponding to the leakage of electrons and photons is 0.65% for the composite dump but the neutron leakage energy should be taken into account. Neutron production and transport in the composite dump have been simulated with the extended MARS10 code [9]. Production of higher energy hadrons in photon-nucleus interactions is not simulated in the frame of the MARS code, but their production rate is much lower and they are important mostly for the thick shielding calculations. It has been found that the percentage of incident energy corresponding to the neutron leakage is 0.08 %. Finally the total leakage from the composite dump is 0.73 % of the incident energy or 375 W. To estimate the direct power deposition in the cooling water a simulation run was made with a 2 cm thick layer of water on the lateral surface of the dump and the result for the power deposition was 19 W.

3.2. Thermal Analysis

The ANSYS code system [12] version 4.4 has been used to calculate temperatures and mechanical stresses in the composite dump. The copper section was omitted in the calculational model. According to the rotational symmetry of the problem the calculations were done in cylindrical coordinates with the z - axis along the dump axis, r - axis along the dump radius and φ - axis corresponds to the azimuthal angle.

An ideal thermal contact was supposed on the boundaries graphite-aluminum and aluminum-aluminum, i.e. the thermal resistance was supposed to be equal zero. All the calculated temperatures are presented for the moment when the equilibrium has been reached and a bunch train has just passed, i.e. they represent the sum of instantaneous and equilibrium temperatures. As material for the core the graphite MPG-6 has been chosen. Thermal and mechanical properties of the MPG-6 graphite and of the aluminum used in the calculations are presented in the tables 3 and 4.

	T [°C]	27	127	327	527	727
aluminum	λ [$Wm^{-1}K^{-1}$]	240	240	230	220	93
	c [$J\,kg^{-1}K^{-1}$]	858	951	1037	1177	1177
graphite MPG-6	λ [$Wm^{-1}K^{-1}$]	114	92	75	70	55
	c [$J\,kg^{-1}K^{-1}$]	568	994	1409	1799	2089

Table 3: Thermal conductivity and specific heat for graphite and aluminum at different temperatures.

	aluminum	graphite MPG-6
ρ [$g\,cm^{-3}$]	2.7	1.71
E [$N\,m^{-2}$]	$7.1 \cdot 10^{10}$	$1.0 \cdot 10^{10}$
α [K^{-1}]	$2.58 \cdot 10^{-5}$	$6.7 \cdot 10^{-6}$
ν	0.33	0.26

Table 4: Mechanical properties of graphite and aluminum.

The cooling system was simulated as a water pipe wound around the dump with a pitch of 10 cm and a pipe cross-section of $S = d \cdot d = 2\ \text{cm} \cdot 2\ \text{cm}$. Assuming that the pipe is soldered to the dump surface and the water flow rate G is about 2 l/s, the pipe to water heat transfer coefficient h can be determined using the criterion

$$hd/\lambda = 0.0024 Re^{0.8} Pr^{0.35}$$

where Re Reynolds number, $Pr = \mu c/\lambda$ Prandtls number and λ, μ and c are the water heat conductivity, viscosity and specific heat, correspondingly.

The heat transfer coefficient between water pipe and aluminum surface is about 0.5-0.7 $\text{Wcm}^{-2}\text{K}^{-1}$. Averaged over the dump surface the effective coefficient is approximately 0.1 $\text{Wcm}^{-2}\text{K}^{-1}$ (including the pipe to wall thermal resistance). This value of the heat transfer coefficient was used in the ANSYS calculations. The temperature of the cooling water was supposed to be 30°C.

The calculated longitudinal temperature distributions are presented in Fig. 5. The maximum temperature in the graphite core is about 390°C, in the Al part on the cylinder axis - 141°C, on the radial boundary between Al and C (r=10 cm) - 101°C, and on the outer Al surface - approximately 65°C. The temperature jump on the boundary Al-water can reach 30-35°C. The thermal resistance between Al and C depends on compression forces and according to [13] the heat transfer coefficient h is 0.03 $\text{Wcm}^{-2}\text{K}^{-1}$ at $P = 3.5$ psi and 0.16 $\text{Wcm}^{-2}\text{K}^{-1}$ at P=35 psi (1psi $\approx$ 0.71 N/cm^2). According to [13] graphite paint on the aluminum surface increases h to 0.08 $\text{Wcm}^{-2}\text{K}^{-1}$ at $P = 3.5$ psi and by 11% at $P = 105$ psi. Therefore the pressure on the boundary must be approximately 20-25 N/cm^2 to increase h up to 0.15-0.18 $\text{Wcm}^{-2}\text{K}^{-1}$. The results of the calculation show that the temperature jump on the boundaries graphite-aluminum due to the boundary thermal resistance can reach 20°C-50°C. Therefore the maximum temperature in the graphite core is actually higher than in the case of ideal thermal contact used in the above ANSYS calculations.

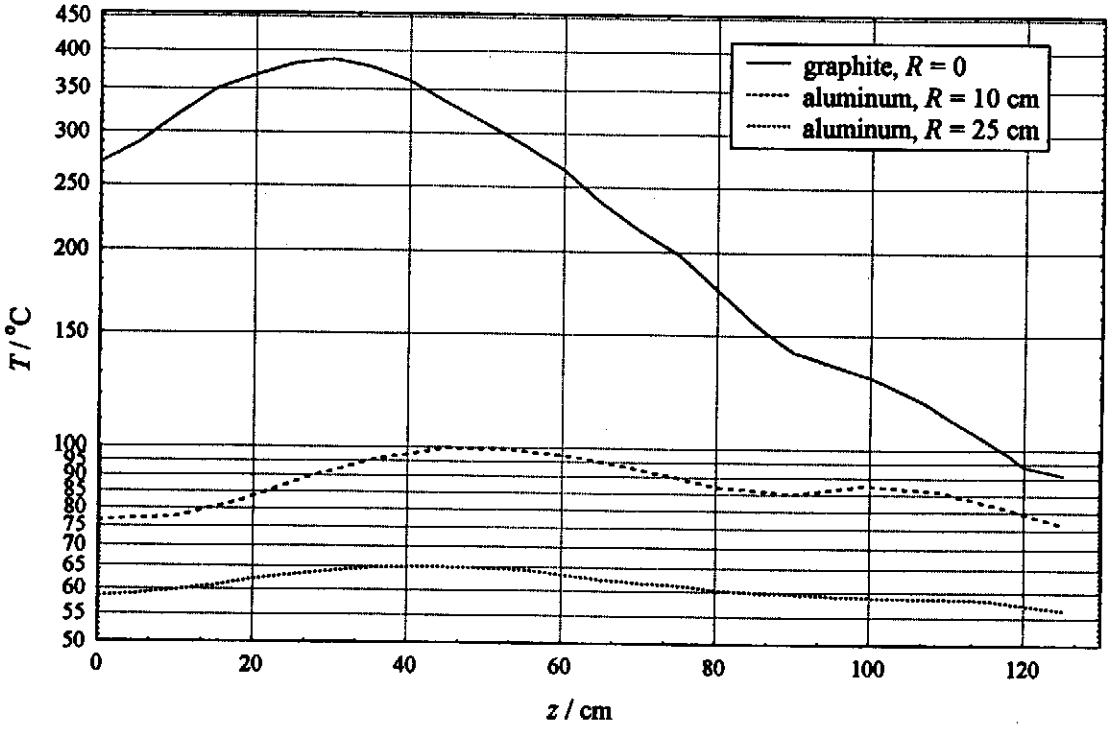

Fig. 5: Longitudinal temperature distributions on the beam axis and on the inner and outer side of the aluminum tube.

To avoid graphite oxidation the graphite surface can be modified by use of silicone, forming a thin film (100-200 μm) of silicone carbide (SiC) on the surface. The linear expansion coefficient of SiC is very close to the linear expansion of MPG-6 graphite and the surface layer will be strong enough both at room and working temperatures.

3. 3 Stress Analysis

Simulations of mechanical stresses in the composite dump were made together with the ANSYS temperature calculations. The stress field was determined in three components in cylindrical coordinates: longitudinal σ_z, radial σ_r and azimuthal σ_φ. The difference between the three stress components is important for estimations of the tolerance value. In the theory of plastic deformation a few criteria are known. For estimating tolerable stresses we use the so called equivalent stress:

$$\sigma_e = \frac{1}{\sqrt{2}}\left((\sigma_r-\sigma_\varphi)^2+(\sigma_r-\sigma_z)^2+(\sigma_z-\sigma_\varphi)^2\right)^{\frac{1}{2}}.$$

The maximum calculated stresses in the graphite are the following:

$\sigma_e = 3365$ N/cm^2,
$\sigma_r = -2403$ N/cm^2,
$\sigma_z = -4444$ N/cm^2,
$\sigma_\varphi = -2403$ N/cm^2.

To reduce these stresses the core can be sectionalized, i.e. it can be separated into graphite tablets with thicknesses from 5 cm to 10 cm. The stress distributions for the case of the sectionalized core are presented in fig. 6 for the tablet with the worst temperatures and stresses. The maximum stresses are the following:

$\sigma_e = 1687$ N/cm^2,
$\sigma_r = -1687$ N/cm^2,
$\sigma_z = -42$ N/cm^2,
$\sigma_\varphi = -1687$ N/cm^2.

The tolerable compression stress for MPG-6 is 9000 N/cm^2 and the tolerable tension strength is 3000 N/cm^2. Therefore MPG-6 graphite can be used in the dump core without problems. To reduce the stresses in the aluminum part it is cut into two pieces - the 125 cm long tube with 20 cm inner diameter; and a 35 cm long plug. In the plug the maximum equivalent stress is $\sigma_e = 5552$ N/cm^2 and in the tube one finds $\sigma_e = 6150$ N/cm^2. Therefore the aluminum material should have a fluidity stress not less than 13000 N/cm^2.

One may worry that the thermal contact between graphite core and outer aluminum tube is lost during operation due to the higher thermal expansion coefficient of aluminum. Radial deformation plots obtained in the assumption that aluminium and graphite parts can move freely in the radial direction are presented in Fig. 7. As a result of the heating a clearance is formed between aluminium and graphite parts at both the beginning and the end of the graphite core. To reduce that clearance a interference fit has to be applied, i.e. the sizes of the graphite tablets have to be chosen such that at working temperature no clearance is formed. Note that the temperature jump equal to 50 °C on the boundary C-Al increases the graphite expansion approximately by 0.03 mm and reduces the clearance.

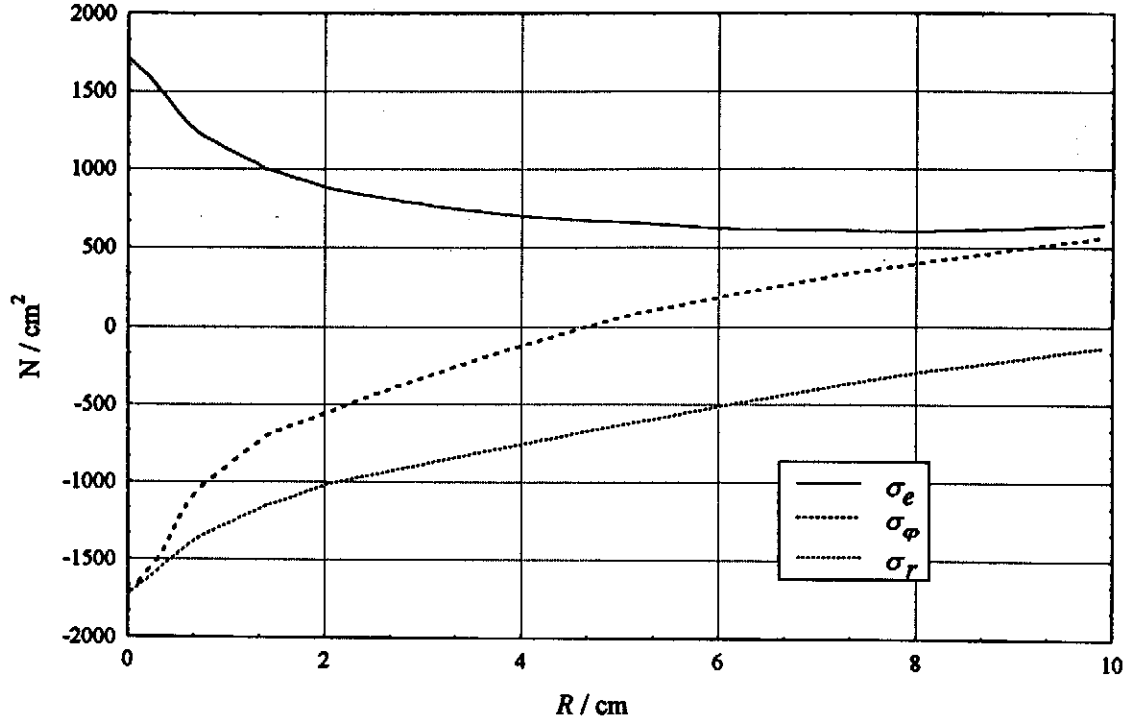

Fig. 6: Transverse stress distributions for the worst tablet in the graphite core.

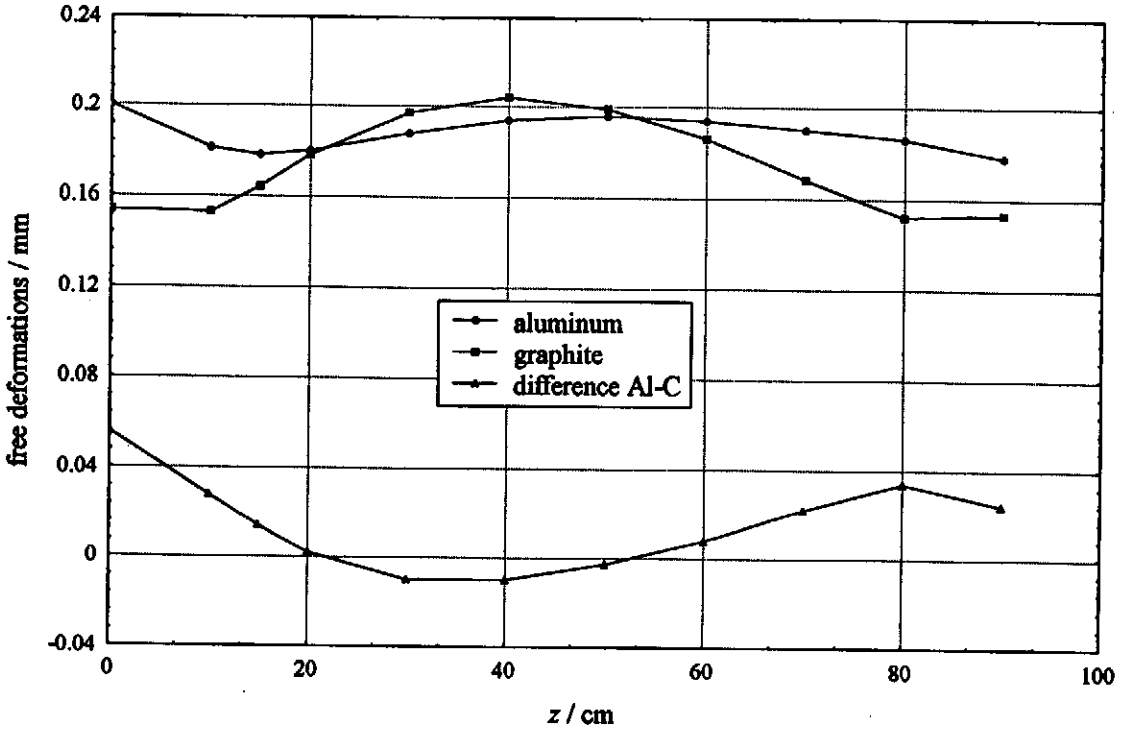

Fig. 7: Transverse deformations due to heating (positive values mean expansion towards larger radii).

4. Residual Radiation and Neutron Dose Shielding

The extended MARS10 code [9] has been used to simulate production and transport of neutrons with energies up to 14.5 MeV generated by the EMS in the composite dump. Production of higher energy hadrons in photon-nucleus interactions is not simulated in the frame of the MARS code. Though their production rate is relatively low compared to the low energy neutrons they are important for estimating the necessary thickness of concrete shielding around the dump (see the below empirical estimations).

The energy spectrum of neutrons leaving the dump is presented in Fig. 8. The convolution of energy dependent neutron fluence with kerma factors [11] is a good estimation of the neutron component of the absorbed dose in any material outside the beam dump. The absorbed doses of radiation in an organic material (CH type) close to the dump surface are shown in Fig. 8. It can be seen that for such high dose rates the radiation hardness of cables, connectors etc. close to the dump is very important.

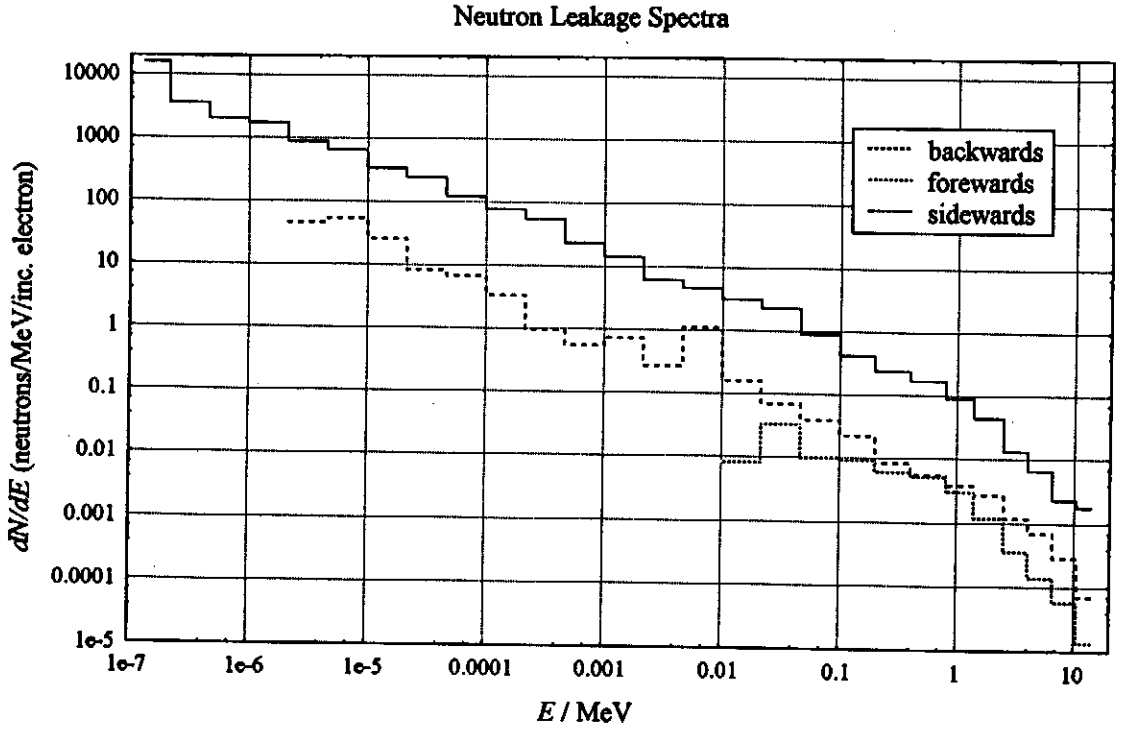

Fig. 8: Energy spectra of leaking neutrons in the low energy region.

Among the variety of radionuclides produced by neutrons and photons in the dump materials the most important are the gamma-radioactive nuclides with a relatively long half-life period $T_{1/2}$. Their number is relatively small : Na^{24} with $T_{1/2} = 15$ hours produced in the reaction $Al^{27}(n,\alpha)Na^{24}$; Cu^{64} with $T_{1/2} = 12.7$ hours produced in the reaction $Cu^{63}(n,\gamma)Cu^{64}$; and Co^{60} with $T_{1/2} = 5.27$ years produced in the reaction $Cu^{63}(n,\alpha)Co^{60}$. The space and time distribution of the residual dose rate is expected to be complicated for a short time t_{sd} after shutdown when the dose rate is very high. A very crude estimation of the residual dose rate near the dump can be made by taking into account the three above mentioned radionuclides only. The properties of the radionuclides and the reaction cross-sections are taken from [11]. The dose rate at 50 cm distance from the dump radial surface and at 50 cm from the downstream plane after one year of the dump operation are presented in table 5. The radioactivation of the cooling water does not seem to be a big problem, but the products of the pipes corrosion contained in the water can become very radioactive.

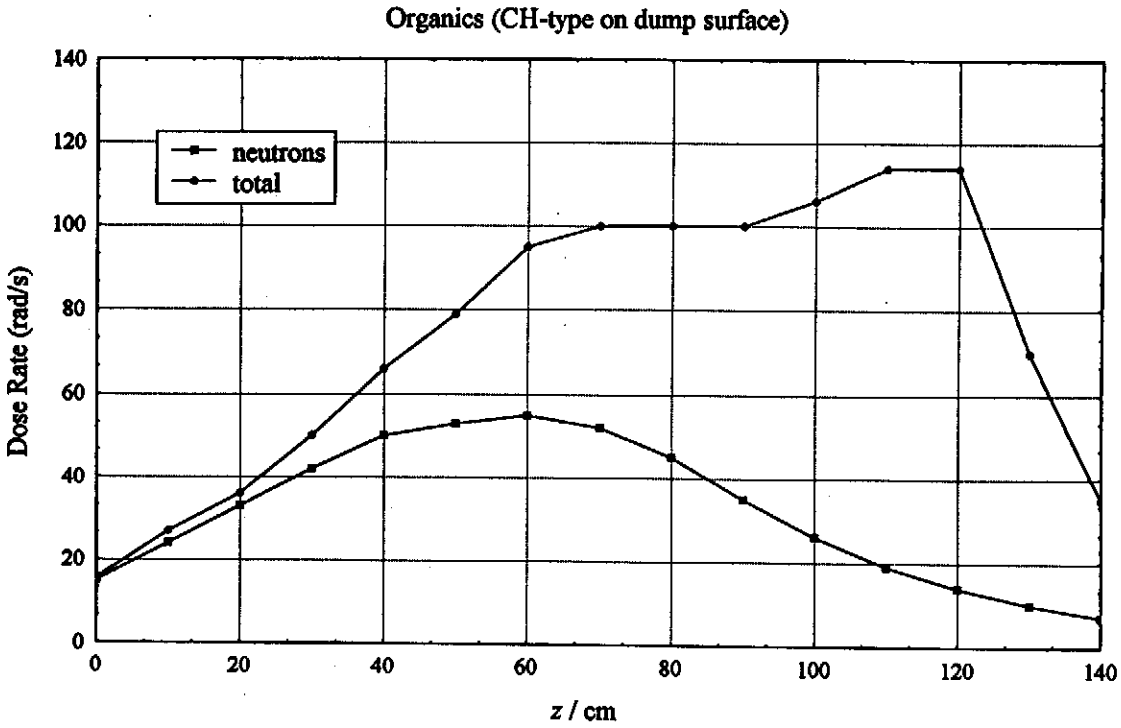

Fig. 9: Dose rates for organic materials on the dump surface during operation at the nominal parameters.

Residual dose rate [mrem/hour]		
t_{sd} [days]	z = 70 cm, r = 75 cm	z = 190, cm r = 0
1	2300	510
3	240	75
7	23	40
30	20	40
365	18	35

Table 5: Residual dose rates as a function of time in the vicinity of the dump.

During operation the beam dump becomes a rather intense source of high energy neutrons as well. Therefore the dump block has to be shielded with concrete in order to reduce the radiation to an acceptable level. The goal should be a reduction below $1..2 \cdot 10^{-5}$ Sv/h in all directions around the dump. In that case there is no need for a so called controlled area. The dose rate behind a concrete shielding can be estimated using a parameterization of Tesch [14]:

$$H = \frac{dN}{dt}\frac{H_0 E_0}{d^2} exp\left(-\frac{d}{\lambda}\right), \qquad (10)$$

where dN/dt is the beam current in particles per second,
d is the shielding thickness,
$H_0 = 1.2 \cdot 10^{-16}$ Sv an empirical constant for graphite,
$\lambda = 0.27$ m for heavy concrete (0.42 m for ordinary).

In Fig. 10 the residual dose rate of the dump absorber is plotted as a function of shielding thickness. We can conclude that one needs 3.5 m of heavy concrete for the absorber.

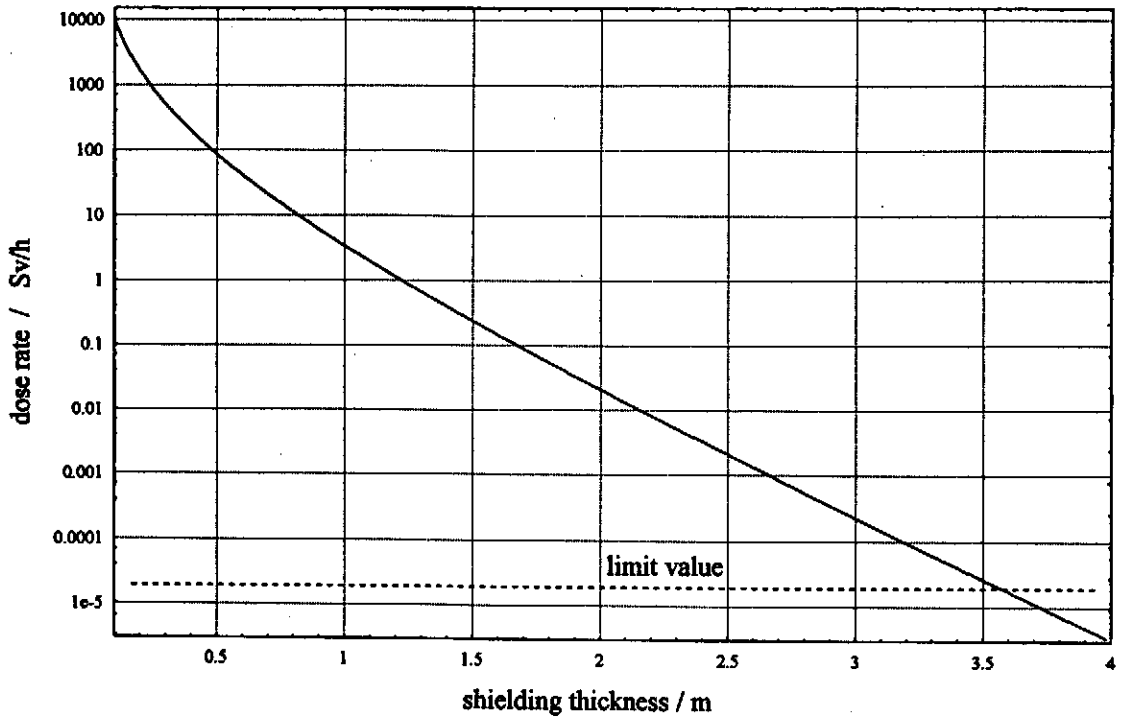

Fig. 10: Dose rate behind shielding by heavy concrete for absorber and spoiler as a function of shielding thickness.

5. Conclusions

The conceptual design of a beam dump which meets the requirements of the TESLA and S-Band test-facilities has been presented. Basically the beam dump has a cylindrical shape and consists of a graphite core insight an aluminum tube followed by an aluminum and a copper section. The design has been investigated with shower simulations and numerical temperature and stress calculations. The simulations show tolerable values of temperatures and stresses for the nominal beam parameters. The total radiation leakage can be kept below 1 percent of the beam power. For a sufficient shielding of the beam induced neutron flux one needs at least 3.5 m of heavy concrete around the absorber.

The proposed design has several special advantages:
- The graphite material exhibits a high temperature and stress resistivity and can accept the unspoiled TTF beam with an rms radius of 1.5 mm. Therefore there is no need to increase the beam spot with an additional spoiler in the beam line as it would have been necessary in case of different materials like aluminum.
- Water cooling of the dump at the radial surface is sufficient. There is only a negligible amount of direct power deposition in the water which avoids problems with hydrogen production and activation of the water cooling circuit.
- The proposed design can be easily modified for use at higher beam energies which will be necessary if the TTF linac is used as a FEL driver. In that case the dump can be filled with pyrolytic graphite or even silicated graphite, materials which exhibit higher densities than ordinary graphite.

6. References

[1] D.R. Walz, L.R. Lucas, The Sphere Dump - A new Low Cost High-Power Beam Dump Concept, SLAC-Pub. 555 (1969)

[2] G. Dimmer, Entwurf der Strahlfänger für MAMI B, diploma thesis (1988)

[3] D.R. Walz, A. McFarlane, E. Lewandowski, Beam Dumps, Stoppers and Faraday Cups at the SLC, SLAC-Pub. 4967 (1989)

[4] C. Sinclair, private communication on the CEBAF beam dump (1994)

[5] E. Carlier et al, The LEP Beam Dumping System, CERN SL/94-49 (1994)

[6] G. Grindhammer, M. Rudowicz, S. Peters, The Fast Simulation of Electromagnetic and Hadronic Showers, Nucl. Instr. & Methods, A290 (1990) 469 - 488

[7] P. Sievers, Elastic Stress Waves in Matter due to Rapid Heating by an Intense High-Energy Particle Beam, CERN BT/74-2 (1974)

[8] I.S. Baishev, N.V. Mokhov. Space Distributions of Electron-Photon Shower Energy Deposition. Preprint IHEP 79-124, Serpukhov (1979).

[9] I.S. Baishev, I.A. Kurochkin, N.V. Mokhov. Extension of the MARS10 Code System Possibilities. Preprint IHEP 91-118, Protvino (1991).

[10] Handbook "Fizicheskie Velichiny". Energoatomizdat, Moscow (1991).

[11] Caswell R.S., Coyne J.J., Randolf M.L. Kerma Factors for Neutron Energies below 30 MeV. Radiation Research 83, 217-254 (1980).

[12] ANSYS, User Manual, Swenson Analysis Systems Inc. (1983)

[13] J.Kidd, N.Mokhov, T.Murphy, M.Palmer, T.Toohing, A High Intensity Beam Dump for the Tevatron Beam Abort System, PAC IX, Washington (1981)

[14] K. Tesch, Shielding Against High Energy Neutrons from Electron Accelerators - a Review, Radiation Protection Dosimetry, Vol. 22/1 (1988) 27 - 32

APPENDIX

Table A1: Energy deposition density (GeV/g/inc.electr., .123-4 ≡ $1.23 \cdot 10^{-5}$).

carbon/aluminum section

r (cm)	0.-0.1	0.1-0.3	0.3-1.	1.-2.	2.-5.	5.-10.	10.-15.	15.-20.	20.-25.
Z (cm)									
0.-5.	.108-1	.492-2	.114-3	.124-5	.508-7	.970-8	.464-8	.876-9	.278-9
5.-10.	.107-1	.553-2	.197-3	.590-5	.271-6	.253-7	.111-7	.293-8	.602-9
10.-15.	.936-2	.532-2	.358-3	.158-4	.939-6	.511-7	.168-7	.405-8	.161-8
15.-20.	.711-2	.470-2	.547-3	.306-4	.207-5	.897-7	.272-7	.584-8	.136-8
20.-25.	.505-2	.373-2	.712-3	.541-4	.373-5	.172-6	.338-7	.106-7	.231-8
25.-30.	.335-2	.285-2	.786-3	.877-4	.596-5	.270-6	.479-7	.112-7	.308-8
30.-35.	.222-2	.203-2	.755-3	.120-3	.909-5	.414-6	.674-7	.165-7	.448-8
35.-40.	.180-2	.158-2	.680-3	.147-3	.124-4	.597-6	.804-7	.179-7	.577-8
40.-45.	.118-2	.116-2	.599-3	.157-3	.158-4	.785-6	.894-7	.203-7	.651-8
45.-50.	.767-3	.894-3	.499-3	.159-3	.182-4	.104-5	.120-6	.296-7	.812-8
50.-55.	.720-3	.674-3	.416-3	.154-3	.204-4	.128-5	.146-6	.314-7	.102-7
55.-60.	.553-3	.544-3	.336-3	.143-3	.217-4	.147-5	.170-6	.402-7	.122-7
60.-65.	.438-3	.421-3	.260-3	.128-3	.226-4	.163-5	.207-6	.459-7	.102-7
65.-70.	.357-3	.316-3	.217-3	.107-3	.217-4	.178-5	.213-6	.500-7	.146-7
70.-75.	.284-3	.274-3	.182-3	.891-4	.205-4	.185-5	.260-6	.493-7	.137-7
75.-80.	.275-3	.219-3	.152-3	.787-4	.193-4	.196-5	.276-6	.523-7	.163-7
80.-85.	.178-3	.155-3	.126-3	.662-4	.177-4	.204-5	.287-6	.683-7	.189-7
85.-90.	.157-3	.139-3	.102-3	.564-4	.164-4	.210-5	.303-6	.696-7	.220-7

aluminum section

90.-92.5	.209-3	.153-3	.952-4	.538-4	.159-4	.206-5	.309-6	.817-7	.306-7
92.5-95.	.172-3	.146-3	.109-3	.549-4	.164-4	.212-5	.303-6	.797-7	.253-7
95.-97.5	.159-3	.150-3	.105-3	.546-4	.159-4	.215-5	.304-6	.693-7	.244-7
97.5-100.	.180-3	.143-3	.938-4	.519-4	.150-4	.203-5	.302-6	.815-7	.245-7
100.-102.5	.122-3	.870-4	.482-4	.140-4	.197-5	.290-6	.727-7	.219-7	.132-3
102.5-105.	.107-3	.784-4	.425-4	.130-4	.184-5	.279-6	.761-7	.220-7	.113-3
105.-110.	.877-4	.864-4	.630-4	.350-4	.111-4	.169-5	.289-6	.748-7	.210-7
110.-115.	.509-4	.473-4	.432-4	.283-4	.887-5	.160-5	.278-6	.729-7	.215-7
115.-120.	.313-4	.312-4	.311-4	.203-4	.731-5	.134-5	.254-6	.679-7	.232-7
120.-125.	.247-4	.245-4	.245-4	.152-4	.542-5	.103-5	.242-6	.678-7	.218-7

copper section

125.-126.	.253-4	.250-4	.245-4	.151-4	.558-5	.107-5	.260-6	.689-7	.234-7
126.-127.	.250-4	.249-4	.249-4	.150-4	.506-5	.102-5	.244-6	.702-7	.120-7
127.-128.	.195-4	.194-4	.193-4	.122-4	.411-5	.882-6	.180-6	.541-7	.128-7
128.-129.	.140-4	.136-4	.130-4	.992-5	.355-5	.692-6	.139-6	.402-7	.117-7
129.-130.	.107-4	.107-4	.106-4	.809-5	.294-5	.632-6	.107-6	.347-7	.130-7
130.-132.	.993-5	.979-5	.780-5	.565-5	.209-5	.435-6	.901-7	.261-7	.842-8
132.-135.	.540-5	.539-5	.538-5	.266-5	.120-5	.232-6	.571-7	.134-7	.444-8
135.-137.	.285-5	.282-5	.281-5	.153-5	.671-6	.139-6	.254-7	.110-7	.331-8
137.-140.	.113-6	.105-5	.103-5	.851-6	.305-6	.679-7	.182-7	.409-8	.123-8